
MobCLIP: Learning General-purpose Geospatial Representation at Scale

Ya Wen*

The University of Hong Kong
Hong Kong, China
wenya@connect.hku.hk

Jixuan Cai*

WeChat, Tencent
Shenzhen, China
codyjxcai@tencent.com

Qiyao Ma

The University of Hong Kong
Hong Kong, China
qyma@connect.hku.hk

Linyan Li

City University of HK
Hong Kong, China
linyanli@cityu.edu.hk

Xinhuan Chen

WeChat, Tencent
Shenzhen, China
holidaychen@tencent.com

Chris Webster

The University of Hong Kong
Hong Kong, China
cwebster@hku.hk

Yulun Zhou †

The University of Hong Kong
Hong Kong, China
yulunzhou@hku.hk

Abstract

Representation learning of geospatial locations remains a core challenge in achieving general geospatial intelligence. Current embedding methods often lack versatility, limiting their utility across diverse tasks in both human and natural domains. We present MobCLIP, the first nationwide general-purpose location encoder, integrating an unprecedented diversity of data modalities through effective and scalable multimodal fusion. Adopting a novel CLIP-based architecture, our framework aligns 100M+ POIs, nationwide remote sensing imagery, and structured demographic statistics with a billion-edge mobility graph. By tokenizing spatial locations into grid cells inspired by Vision Transformers, we establish a unified representation space bridging mobility patterns and multimodal features. To rigorously evaluate the general-purpose effectiveness of MobCLIP, we construct a benchmark dataset composed of 11 downstream prediction tasks across social, economic, and natural domains. Experiments show that MobCLIP, with four input modalities and a compact 128-dimensional representation space, achieves significantly superior general-purpose predictive performances than state-of-the-art models by an average of 35%. Thanks to the effective integration of human-centric modalities, the performance gain is particularly profound in human-centric tasks, such as energy consumption (+260%), offline retail consumption amount (+98%), and crime cases (+95%) predictions. Echoing LLM scaling laws, we further demonstrate the scaling behavior in geospatial representation learning. We open-source code and pretrained models at: <https://github.com/ylzhouchris/MobCLIP>.

*Equal contribution. Work done when Ya Wen was an intern at Tencent.

†Corresponding Author.

1 Introduction

Geospatial representation learning is crucial for enabling AI systems to understand and reason about spatial patterns, relationships, and dynamics across diverse geographic contexts [6, 54, 28]. This process involves encoding regions into low-dimensional vectors that capture both their intrinsic characteristics and their correlations. Despite some early attempts [43, 20, 39], the lack of large-scale general-purpose region representations remains a fundamental bottleneck.

There has been a rise in geospatial representation learning studies, attempting to construct pretrained information-dense spatial representations for specific downstream tasks. Wu *et al.* [42] established a unified location encoding framework that consolidates 15 commonly recognized location encoders that mainly come in two folds. Position encoding functions [26] maps 2D coordinates into high-dimensional feature space using ideas such as spherical harmonics [26] and sinusoidal activations [33]. Early attempts of self-supervised location embeddings methods primarily combine image data, either geo-tagged photos or satellite imagery, with geospatial locations using contrastive learning models [38, 25, 19]. These methods demonstrate the potential of "clipping" contextual information to geospatial regions, achieving success in downstream tasks like global localization [38].

However, geospatial inference tasks are inherently multimodal in nature. Effective and scalable representation learning requires careful selection, alignment, and integration of multiple informative input modalities. Mobility data, for instance, captures human behaviors in cities, with mobility graphs enhancing correlations between locations through movement patterns. While studies have shown the effectiveness of mobility graphs at city scales [56, 46, 51, 52], demographic statistics have also proven valuable in urban representation learning [40]. Among these attempts, the contrastive learning framework and the CLIP [31] model has become prominent in multimodality alignment. The difficulty of effective multimodal fusion increases dramatically with the number of input modalities. Multimodal alignment for geospatial data remains a challenge.

Geospatial representations, if learned well, should demonstrate superior general-purpose inference capabilities in a variety of downstream tasks spanning social, economic, and natural prediction domains. Existing methods [26, 19] focus primarily on natural tasks such as forest coverage estimation, elevation estimation, and bird species classifications [25], paying insufficient attention to human-centric tasks related to the social-economic dynamics essential in global cities. There is a lack of comprehensive benchmarks involving both human-centric and natural tasks, making it difficult to evaluate the general-purpose inference capabilities of location encoders.

To address these challenges, we propose MobCLIP, the first nationwide general-purpose location encoder that integrates an unprecedented diversity of data modalities through a scalable multimodal fusion framework. Unlike traditional methods, MobCLIP innovatively leverages mobility data as the backbone, fusing information from other modalities into it using a CLIP-based approach. This strategy not only improves multimodal integration but also explicitly addresses the traditional underemphasis on human-centric data. Our contributions can be summarized as follows:

- We introduce MobCLIP, the first nationwide, general-purpose pretrained location encoder, designed for diverse tasks beyond traditional geospatial domains.
- We introduce the novel use of mobility data as the backbone, combined with a self-supervised multimodal pretraining framework, thereby emphasizing the significance of human-centric information in geospatial learning.
- We construct a benchmark dataset of 11 downstream prediction tasks spanning social, economic, and natural domains for performance evaluation. Extensive experiments show that our model achieves significantly superior performance—improving by over 35% on average—across all general-purpose tasks. Performance gains are especially profound in human-centric tasks.
- We open-source our methodology, a distilled version of MobCLIP, and a **benchmark dataset** for general-purpose evaluation to advance research on general-purpose pretrained location encoders.

2 Related Works

Pretrained foundation model for general geospatial inference. Geospatial data is inherently diverse and multimodal, comprising various forms such as maps [41, 2, 8], texts [21, 22, 11], images [10, 14], and graphs [43, 39], all of which have been widely employed to advance the understanding

of urban areas. To effectively leverage this diversity, multimodal region representation learning has emerged as a paradigm for integrating cross-modality information in a self-supervised manner to learn task-agnostic regional embeddings [47, 53, 52, 51]. However, such frameworks require each city to be trained individually while heavily relying on the availability of multimodal data in the study area, resulting in limited generalizability. Following the success of pretrained Foundation Models (FMs) in language and vision domains, there is increasing interest and active discussion around developing foundation models for geospatial artificial intelligence (GeoAI) [27, 54]. ReFound [45], one of the early attempts, aims to distill extensive knowledge from general FMs while incorporating domain-specific objectives for enhanced performance. It collects POI and satellite image data from five major cities in China as the pretraining corpora, which is relatively limited in scope and diversity of data modalities compared to ours. Perhaps the one most similar to us in concept is the Population Dynamics Foundation Model (PDFM) [1], which encodes postal codes and counties across the United States into embeddings by aggregating features such as busyness and search trends via a neighborhood-based graph. However, comparatively, it still falls short in the richness and diversity of modalities. Additionally, the model adopts simple concatenation for cross-modality fusion and relies solely on geographical proximity for information aggregation, missing the higher-level correlations captured by our mobility graph.

Position encoding functions. A straightforward approach for representing geolocations involves using analytical transformations to convert 2D or 3D coordinate inputs into higher-dimensional vectors while ensuring that the resulting embeddings preserve the geographical distances between locations. For instance, Space2Vec [24] encodes locations using sinusoid functions with different frequencies in a 2D Euclidean space. Extending from 2D space, Neural Radiance Fields (NeRF) [29] encodes continuous 3D coordinates via Fourier input mapping. To further account for the Earth’s spherical geometry, Sphere2Vec [26] and Siren [33] introduce specialized position encoders designed to capture spherical distances between coordinates. The position encoders are typically followed directly by a neural network, which is trained in a supervised manner on task-specific datasets.

Self-supervised location representation pretraining. To reduce reliance on heavily labeled data, which is both scarce and costly to obtain, and to leverage the abundance of unlabeled geo-tagged and satellite images [49, 50, 48], self-supervised pretraining methods have emerged for location representation learning. Contrastive Spatial pretraining (CSP) [25] learns location embeddings from unlabeled imagery using a contrastive objective. CSP is pretrained, fine-tuned, and tested on the same datasets (i.e., iNat2018 [37] and fMoW [9]), without demonstrating generalizability to other tasks. SatCLIP [19] and GeoCLIP [38] both pretrain location encoders via contrastive learning on coordinate-image pairs to generate global location embeddings. Their primary differences lie in the architectures of their location and image encoders, as well as the pretraining datasets used. Although existing location-based pretraining methods excel in enabling global-scale embedding queries, they fail to incorporate other geospatial modalities beyond images and overlook crucial factors, such as human activities, that are essential for learning general-purpose location representations.

3 Methodology

The framework is designed to learn versatile region representations by integrating geospatial features from four distinct modalities: human mobility (modeled as a graph), Points-of-Interest (POIs) as textual data, satellite imagery as visual input, and demographic distributions represented as tabular categorical histograms. Figure 1 illustrates the proposed methodological framework.

3.1 Mobility as the Backbone

Geographic location serves as a precise anchor for aligning multimodal data. Prior region embedding methods [42, 19] often rely on coordinates to fuse different modalities, but this limits the inclusion of network-based signals. Human activity frequently spans geographic boundaries via transport or digital networks, and mobility data—represented as links in a spatial graph—captures these non-local patterns. We propose to use the mobility graph as a backbone for multimodal fusion in geospatial representation learning.

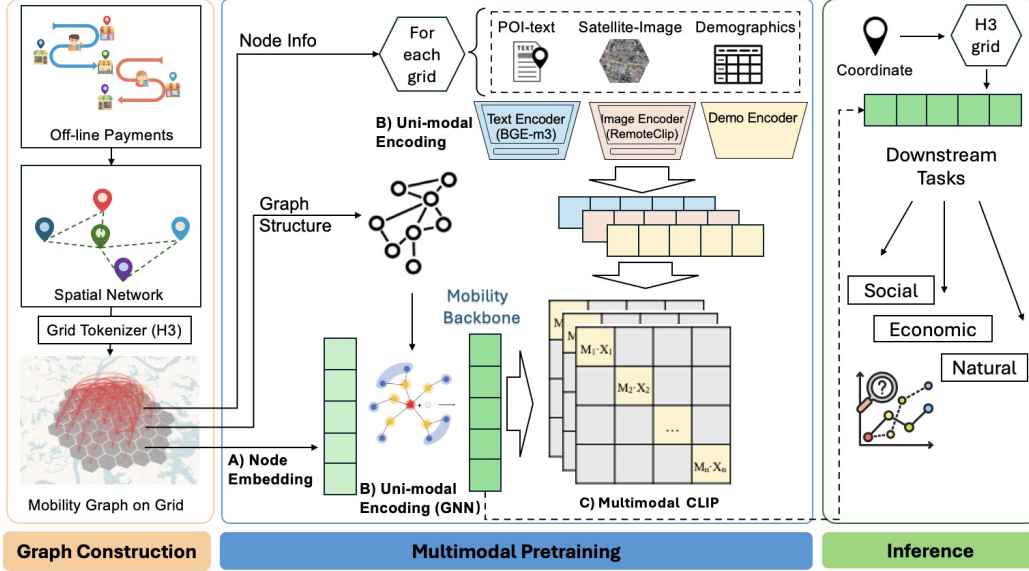


Figure 1: The methodological framework of MobCLIP.

Tokenizing Locations for Graph. Raw spatial interactions are sparse and misaligned in time and space, making coordinate-based graphs too fragmented to reflect major flows. Inspired by Vision Transformers (ViT) [18], which partition images into patches, we grid geographic space and build graphs at the cell level. We adopt the H3 grid [36], which minimizes distortion compared to Geohash and Google S2 [3], offering balanced global coverage. At level 6 ($\sim 36 \text{ km}^2$ per cell), we construct a nationwide mobility graph from real-world transaction data as presented in the “Graph Construction” section in Figure 1. This large-scale network captures human movement patterns and serves as the backbone for multimodal alignment and representation learning.

Pre-encoding. We utilize LINE (Large-scale Information Network Embedding) [34] to preprocess the full mobility graph and generate 128-dimensional embeddings for each H3 grid cell. Based on empirical evaluation, we select LINE embeddings with second-order proximity, which offer superior performance. When paired with the graph sampling strategy described below, this approach effectively preserves the information from the full mobility graph with minimal computational effort.

Graph-based mobility encoder. Graph Neural Networks (GNNs) have proven to be effective frameworks for capturing relationships between nodes, taking into account high-order dependencies. GNNs operate through a message-passing mechanism, where each node updates its representation by aggregating information from its neighboring nodes. To encode a graph \mathcal{G} using L layers of GNNs, the l^{th} layer embedding of a node i is computed as follows:

$$e_i^{(l)} = \text{AGG} \left(e_i^{(l-1)}, \{e_j^{(l-1)} \mid j \in \mathcal{N}_i\} \right) \quad (1)$$

where \mathcal{N}_i refers to the neighborhood of the node i , and $\text{AGG}(\cdot)$ is the aggregation function, which can vary across different models. In our framework, we employ LightGCN [12] as our mobility graph encoder. It simplifies the traditional GNN architecture by removing unnecessary feature transformation and nonlinear activation, and only keeping the most essential component: neighborhood aggregation. In LightGCN, node features are initialized as learnable parameters and by utilizing L layers of propagation, it generates $L + 1$ distinct embeddings for each node, namely $(e^{(0)}, e^{(1)}, \dots, e^{(L)})$:

$$e_i^{(l+1)} = \sum_{j \in \mathcal{N}_i} \frac{1}{\sqrt{|\mathcal{N}_i|}} e_j^{(l)} \quad (2)$$

The final embeddings are computed by summing all layer embeddings:

$$\mathbf{e}_i = \sum_{k=0}^K e_i^{(k)} \quad (3)$$

We use the pre-encoded LINE embeddings to initialize the node features and construct a mobility subgraph as the graph encoder input. This subgraph is extracted from the full graph using a *top-k* sampling strategy based on a percentage threshold, ensuring that the links with the highest flows are retained for each node. This strategy aims to address the "long-tail" distribution patterns commonly seen in geospatial studies, where a small number of regions experience very high flows, while the majority of regions exhibit significantly lower flows that have minimal impact on the overall graph structure. We adopt a top sampling ratio of 10% for the main experiments.

3.2 Auxiliary Multimodality Encoder

For general-purpose geospatial inference, the selection of fundamental input modalities that are (1) effective for a variety downstream tasks in both human-centric and nature domains, and (2) complementary to each other, is critical for the performance multimodal representation learning. Based on existing knowledge from spatial data science and urban studies and demonstrated effectiveness in literature, we select three fundamental auxiliary modalities to complement the mobility backbone, including Point-of-Interest (POI), Demographic Statistics, and Satellite imagery.

Different unimodal encoders are selected to encode auxiliary modalities. **(1) Point-of-Interest (POI):** We encode both POI categorical statistics and textual information using language models [7]. Specifically, we use the BGE-m3 model [5] to encode both POI names and categories. Embedding of all POIs located within each H3 grid was then averaged to be the grid embedding. **(2) Satellite imagery:** We use an off-the-shelf pretrained image encoder, RemoteClip [23], to generate image embeddings for each H3 grid. **(3) Demographic Statistics:** The categorical demographic data in tabular form is encoded using an MLP-based encoder.

3.3 Multimodality Alignment with Mobility

We adopt a CLIP-inspired contrastive learning scheme to jointly project embeddings of the four modalities into a joint embedding space and aligned under a contrastive learning objective.

We train our model using a CLIP-inspired contrastive learning scheme, in which mobility serves as the central modality that other modalities align to. We construct modality tuples $(\mathcal{M}, \mathcal{I}, \mathcal{T}, \mathcal{D})$ for all grids in the study area, where \mathcal{M} indicates mobility, and $\mathcal{I}, \mathcal{T}, \mathcal{D}$ represent images, texts, and distribution data, respectively. Given the mobility feature \mathbf{m}_i of a grid and its corresponding observations in other modalities $\mathbf{I}_i, \mathbf{t}_i, \mathbf{d}_i$, we encode them into normalized embeddings by modality-specific encoders: $f(\mathbf{m}_i) \in \mathbb{R}^d$ and $g(\mathbf{x}_i) \in \mathbb{R}^d$ where $\mathbf{x} \in \{\mathbf{I}, \mathbf{t}, \mathbf{d}\}$. Specifically, f is a graph neural network, whereas g are pretrained foundation models for texts and images (see Section 3.2), and an MLP for demographic categorical features. The encoders are optimized with the objective

$$\mathcal{L} = \frac{1}{|\{\mathcal{I}, \mathcal{t}, \mathcal{d}\}|} \sum_{\mathcal{X} \in \{\mathcal{I}, \mathcal{t}, \mathcal{d}\}} (\mathcal{L}_{\mathcal{M}, \mathcal{X}} + \mathcal{L}_{\mathcal{X}, \mathcal{M}}) \quad (4)$$

where the three assisting modalities are aligned with mobility individually and simultaneously by

$$\mathcal{L}_{\mathcal{M}, \mathcal{X}} = \frac{1}{2N} \sum_{i=1}^N -\log \frac{\exp(\langle f(\mathbf{m}_i), g(\mathbf{x}_i) \rangle / \tau)}{\sum_{j=1}^N \exp(\langle f(\mathbf{m}_i), g(\mathbf{x}_j) \rangle / \tau)} \quad (5)$$

which maximizes the similarity between a grid's mobility features and its corresponding POI, image, or demographic features, while minimizing the similarity to these features of other grids within the same batch $(\mathbf{m}_i, \mathbf{x}_i)_{i=1}^N$, and a symmetric loss $\mathcal{L}_{\mathcal{X}, \mathcal{M}}$ doing the other way around. $\langle \cdot, \cdot \rangle$ represents the dot product operation and τ is a temperature parameter adjusting the smoothness of the logits in the softmax.

4 Experiments

4.1 Experimental Settings

4.1.1 Multimodal Pretraining

Mobility dataset. We construct a store-level network based on consumer mobility from WeChat Pay, a nationwide electronic transaction platform in China operated by Tencent, with extensive

offline payment coverage. Each offline store is mapped to an H3 grid cell based on its geographic coordinates. If a user makes purchases at stores in different grids within the same week, an undirected, weighted edge is formed between the corresponding grid cells, generating a weekly mobility graph. Aggregating data over 54 weeks and 50 million unique stores yields a large-scale graph at H3 resolution level 6, with approximately 200,000 nodes and 1.2 billion edges. This nationwide graph captures fine-grained human movement patterns and serves as the foundational mobility graph.

Auxiliary modality datasets. More than 100 million Points-of-Interest (POIs) are collected from Tencent Maps, including both their names and category labels. POI names are typically short, referring to store names, company names, or types of public facilities. The POIs span 445 distinct categories [35]. For each POI, we concatenate its name and category, and encode the combined text using a pretrained text embedding model. In terms of images, we obtain Google Satellite imagery with a resolution of approximately 10 meters (at zoom level 14) for each H3 grid. Grid-level demographic statistics are processed by aggregating population structure data from WorldPop [44]. Each H3 grid records the population count by age group (5-year intervals) and gender in 2020.

Implementation details. We split the dataset into 90% for training and 10% for validation to mitigate overfitting. The model is trained for 100 epochs with a batch size of 20,480, using the Adam optimizer with a learning rate of 0.001 and weight decay of 0.001 on a single NVIDIA A100 GPU for one hour. During training, we conduct a grid search over commonly used hyperparameters: learning rate $\in \{1e-4, 2e-4, 5e-4, 1e-3, 2e-3, 5e-3\}$ and weight decay $\in \{1e-3, 1e-2, 1e-1\}$. A comprehensive list of tuned hyperparameters is provided in our supplementary GitHub repository. The LINE embedding for nationwide mobility graph was processed at Tencent’s Angel distributed graph computing platform [15], utilizing hundreds of computing cores and the embedding of over a billion edges is completed efficiently within a few hours.

4.1.2 General-purpose Evaluation

Downstream tasks and datasets. To assess the generalizability of our model, we curated a set of 11 downstream tasks as shown in Table 1. These tasks were selected for their diversity and broad representativeness, covering three key domains: social, economic, and natural. They are evenly distributed across China, ensuring that the evaluation is free from geographic bias. In addition, considering the influence of statistical unit delineation in geospatial analysis, the downstream tasks are designed to span four distinct spatial scales — point, grid, county/district, and city/prefecture — to examine the impact of resolution effect in region representation learning. MobCLIP is trained at the H3 grid level. For point-level tasks, the embedding corresponding to the grid containing the point is extracted for evaluation. For administrative-level tasks, we compute the mean embedding of all grids within the administrative unit, which is then used to assess regression performance. This multi-scale evaluation further validates the generalizability of the model across varying spatial resolutions. The data sources are listed in the table and are primarily derived from WorldPop [4], MOSAIKS [32], and 2020 China Census Year Book [30]. Additionally, ENE (energy consumption) was collected from various local statistical yearbooks. The total energy consumption of one city/prefecture is calculated by converting different forms of energy usage into tonnes of standard coal equivalent. As this work has not yet been formally published, the data are not publicly available now. Furthermore, another unavailable dataset used in our evaluation is COS (offline consumption amount) from Tencent WeChat Pay, which was used to test whether the embeddings can predict regional consumption indices.

Prediction models. We implement LightGBM [17] as the downstream prediction model. The hyperparameters are lightly tuned, and the average performance on the test set over 10 runs is reported along with the standard deviation. To enhance performance while mitigating the risk of overfitting, different sets of hyperparameters are used for tasks at different levels, considering the variation in sample sizes. For city-level electricity consumption prediction tasks, Ridge regression is adopted due to the limited number of data samples.

4.2 Performance Comparison

Baseline models. We benchmark MobCLIP against the strong existing approaches: 1) Self-supervised pertaining approaches: SatCLIP (with ViT-16) [19], GeoCLIP [38] and CSP [25]; and 2) analytical position encoding functions: Sphere2Vec (sphereC+) [26], Siren [33], and NeRF [29]. (The

Table 1: Summary of datasets for downstream tasks.

Abbreviation	Description	Data Source	Spatial Scale	Publicly Available
Social Tasks				
POP	Population density	WorldPop [4]	Grid	Y
EDU	Average education years	Census Year Book [30]	County/District	Y
ELD	Elderly (65+) population ratio	Census Year Book [30]	County/District	Y
HSR	Hukou separation ratio	Census Year Book [30]	County/District	Y
CRI	Crime cases	[55]	Grid	Y
Economic Tasks				
NTL	Nighttime light intensity	MOSAIKS [32]	Point	Y
HOU	Per capita housing area	Census Year Book [30]	County/District	Y
ENE	Energy consumption	City statistical yearbooks	City/Prefecture	N
COS	Offline consumption amount	Tencent	Grid	N
Natural Tasks				
ELE	Elevation	MOSAIKS [32]	Point	Y
FOR	Forest coverage	MOSAIKS [32]	Point	Y

selection is based on methods’ superior performance reported in previous work [42]). Note that the location encoders used for comparison in this study take 2D coordinates as input, whereas MobCLIP operates on H3 grids as its spatial unit. To ensure consistency, we generate location embeddings for the centroids of the H3 grids for comparison with our grid embeddings.

Comparison results. In Table 2, we compare the prediction performance of MobCLIP against baseline models across a range of tasks and organize the results based on the categories of downstream tasks. Clearly, MobCLIP achieves significantly better results across all human-related tasks, with an average improvement of 35.8% and 87.9% for social and economic tasks, respectively. In the two nature-related tasks (i.e., elevation and forest coverage prediction), SatCLIP performs comparably or slightly better, showing a minor average difference of 4.1 % in prediction performance. Note that both elevation and forest coverage data tend to exhibit gradual and continuous spatial changes, meaning that their variation is often highly correlated with the "absolute" location differences. Hence, it is reasonable that the location encoders with only latitude/longitude as input can capture the patterns well enough. However, the majority of tasks that hold value in practice are related to human behavior, which typically does not exhibit easily inferable location-dependent properties. In such tasks, MobCLIP performs significantly better, showcasing its ability to capture complex, high-level region correlations beyond simple geographic proximity. Meanwhile, the minor performance gap in the two nature-related tasks compared to top-performing methods suggests that our model also effectively captures direct region adjacency along with more nuanced features.

Additionally, the superiority of MobCLIP is consistent across varied spatial scales, achieving the best performance on tasks at city, county, and grid levels. Notably, in the city-level energy consumption task, MobCLIP demonstrates impressive results with a prediction accuracy of 0.72 in terms of R^2 . In contrast, the baseline models exhibit R^2 values fluctuating around zero, failing to capture regional features at coarser resolutions.

4.3 Scaling Behavior in Geospatial Representation Learning

Echoing scaling behaviors observed in LLMs [16], we investigate the scaling of model performance in geospatial representation learning with pretraining data size and spatial coverage. Figure 2 illustrates model performances of three MobCLIP variants, respectively trained using data from three nested spatial coverages, namely *Jiangsu*, *East China*, and *China*. The spatial extents are shown in Figure 2(r). We conducted three separate experiments with different pretraining data sizes. While *Jiangsu* contains 3,904 H3 cells, *East China* contains 28,855 cells and *China* contains 195,574 cells. All three pretrained models are tested in *Jiangsu* only, using evaluation methods described in Section 4.1.2.

We observe that downstream model performance generally increases with increased pretraining data size for both social and economic tasks (Figure 2, Appendix A.2). The performance increase from *Jiangsu* to *East China* is especially large, while the increase from *East China* to *China* is relatively marginal. External training information can be useful for internal predictions. The marginal benefits of increasing training data size gradually decline. The scaling behavior in geospatial representation

Table 2: **Comparison of model performances on 11 downstream tasks spanning social, economic, and natural aspects.** Previous best results are underlined, while best results are highlighted in **bold**. Model performances are measured by R^2 , and the standard deviation over ten repeated trainings are marked in brackets below. Row Δ illustrates the percentage difference between Our Method’s performance and the best baseline.

Model	Dim \downarrow	Social Tasks					Economic Tasks				Natural Tasks		AVG $R^2 \uparrow$
		POP	EDU	ELD	HSR	CRI	NTL	HOU	ENE	COS	ELE	FOR	
State-of-the-art pretrained Location Encoders													
SatCLIP [19]	256	0.52 (0.03)	0.63 (0.01)	0.68 (0.03)	0.74 (0.03)	0.39 (0.01)	0.33 (0.03)	0.66 (0.03)	-0.07 (0.11)	0.44 (0.03)	0.96 (0.00)	0.81 (0.01)	<u>0.55</u>
GeoCLIP [38]	512	0.41 (0.04)	<u>0.66</u> (0.01)	0.66 (0.02)	0.69 (0.03)	0.32 (0.01)	0.24 (0.03)	0.65 (0.02)	0.11 (0.01)	0.32 (0.00)	0.92 (0.00)	0.73 (0.01)	0.52
CSP [25]	256	<u>0.55</u> (0.03)	0.65 (0.02)	0.62 (0.03)	0.68 (0.03)	<u>0.39</u> (0.01)	0.29 (0.03)	0.62 (0.02)	<u>0.20</u> (0.03)	<u>0.46</u> (0.03)	0.95 (0.00)	0.77 (0.01)	<u>0.55</u>
Sphere2Vec [26]	96	0.40 (0.03)	0.56 (0.02)	0.62 (0.04)	0.61 (0.03)	0.34 (0.01)	0.26 (0.03)	0.57 (0.02)	-0.01 (0.01)	0.35 (0.03)	0.95 (0.00)	0.76 (0.01)	0.49
NeRF [29]	96	0.40 (0.03)	0.63 (0.02)	0.61 (0.03)	0.61 (0.03)	0.33 (0.01)	0.24 (0.03)	0.56 (0.02)	0.03 (0.05)	0.33 (0.02)	0.95 (0.00)	0.76 (0.01)	0.50
Siren [33]	1,024	0.51 (0.03)	<u>0.66</u> (0.02)	<u>0.69</u> (0.03)	0.74 (0.03)	<u>0.39</u> (0.01)	0.33 (0.03)	0.66 (0.03)	-0.14 (0.14)	0.44 (0.03)	0.96 (0.00)	<u>0.80</u> (0.01)	0.54
Ours													
MobCLIP	128	0.83 (0.02)	0.85 (0.01)	0.81 (0.02)	0.81 (0.02)	0.81 (0.00)	0.62 (0.02)	0.70 (0.02)	0.72 (0.02)	0.91 (0.01)	0.90 (0.00)	<u>0.80</u> (0.00)	0.75
Δ		+51%	+29%	+17%	+9%	+95%	+88%	+6%	+260%	+98%	-6%	-1%	+35%

learning is consistent with findings in language and vision domains, where model performance improves with scale [13]. Results emphasize the value and necessity of geospatial representation learning at scale. Even for small-scale predictions, an increase in training data size and spatial coverage will introduce relevant information and improve downstream predictive performances.

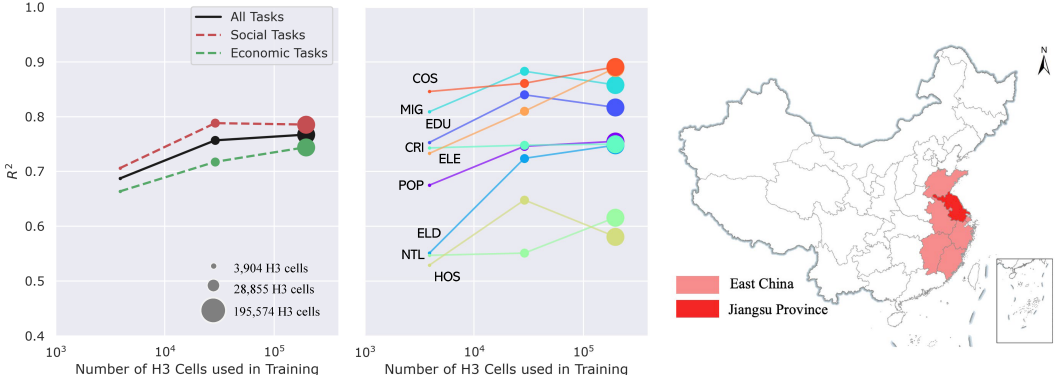


Figure 2: **Scaling behavior of downstream task performance with pretraining data size and spatial coverage.** Map on the right illustrates the spatial extent of Jiangsu Province, East China, and the entire China, respectively covering 3,904, 28,855, and 195,574 H3 cells used for the pretraining. Left figure illustrates average R^2 values for all tasks, social tasks, and economic tasks respectively, while the middle figure illustrates task-specific scaling behaviors. Detailed numbers in Appendix A.2.

4.4 Ablation and Sensitivity Study

Module-wise ablation study. Figure 3(a) shows the performance of multiple model variants on downstream tasks for ablation analysis. First, the CLIP-based multimodal alignment module enriches the model by incorporating complementary information from various modalities. The columns labeled **w/o CLIP** indicate that removing this module leads to an average performance drop of 5% on human-related tasks. More notably, performance on natural-related tasks drops sharply from 85% to 63%, indicating that while mobility data is highly informative, it primarily captures human-centric patterns. In contrast, multimodal inputs—such as remote sensing imagery—provide richer representations of natural features. These results show that integrating diverse modalities leads to a more comprehensive and general-purpose regional representation. Second, mobility forms the backbone of **MobCLIP**, and graph information is integrated at two distinct stages. We evaluate each stage by removing

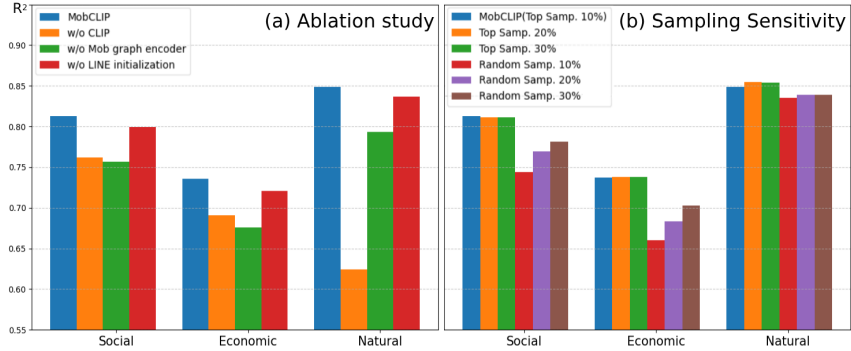


Figure 3: **Model comparison results for ablation studies and sensitivity analysis.**

them individually. When the graph encoder is removed, we replace it with a simple MLP. As shown by **w/o Mob Graph Encoder**, the performance drop is most pronounced on human-related tasks, suggesting the GCN effectively captures human-centric patterns via relational structure. Replacing LINE initialization with random values (**w/o LINE Initialization**) has the smallest impact across task types. This suggests LINE is less effective than GCN in capturing informative structure. However, a consistent 1–2% drop across tasks indicates that LINE still provides complementary value.

Sensitivity to graph sampling. Considering the importance of the mobility graph encoder, we conduct a sensitivity analysis on both the node neighbours sampling strategy and the sampling ratio (Figure 3(b)). We compare our *top-k* sampling approach with random sampling, which retains links randomly based on a percentage threshold instead of depending on link weights. The results suggest that varying the *top-k* sampling ratio has limited effect on performance, as the difference between top 10% and top 30% sampling remains marginal. In contrast, random sampling tends to include nodes from the "tail" of the long-tail distribution, introducing noise that adversely affects model accuracy. As a result, random sampling generally underperforms *top-k* sampling at equivalent ratios. However, as the random sampling ratio increases, the model gradually captures broader and more generalized patterns, while the relative impact of noise diminishes, leading to improved performance. These findings highlight that MobCLIP is a unified framework capable of balancing performance and computational efficiency under different graph configurations.

5 Conclusion

In this work, we present MobCLIP, a general-purpose framework for geospatial representation learning at scale. Centered around a billion-scale mobility graph and enriched with multimodal alignment—including POIs, remote sensing imagery, and tabular data—MobCLIP learns unified region embeddings that generalize across diverse downstream tasks. Extensive experiments on 11 tasks spanning social, economic, and natural domains demonstrate that MobCLIP consistently outperforms existing state-of-the-art methods. Moreover, our findings echo the scaling laws observed in other domains: as the spatial coverage of training data increases from local to national scale, representation quality and task performance improve substantially.

Despite strong empirical results, limitations remain. The scale issue in spatial representation learning is not fully addressed. We conducted a sensitivity analysis to show that MobCLIP is robust over different spatial scales (Appendix A.3). Second, high-quality human mobility data may be difficult to obtain in some regions for obvious privacy concerns. To resolve this issue, we generate and open-source a distilled version of MobCLIP that is free from privacy concerns. Specifically, we train a multi-layer perceptron (MLP) to map continuous geographic coordinates into high-dimensional embeddings, supervised by MobCLIP’s grid-level outputs. This approach not only enables users to retrieve high-quality region embeddings for any arbitrary coordinate, free from privacy concerns, but also removes the dependency on H3-based lookup. Detailed implementation of the distillation approach is provided in Appendix A.1.

References

- [1] Mohit Agarwal, Mimi Sun, Chaitanya Kamath, Arbaaz Muslim, Prithul Sarker, Joydeep Paul, Hector Yee, Marcin Sieniek, Kim Jablonski, Yael Mayer, et al. General geospatial inference with a population dynamics foundation model. *arXiv preprint arXiv:2411.07207*, 2024.
- [2] Pasquale Balsebre, Weiming Huang, Gao Cong, and Yi Li. City foundation models for learning general purpose representations from openstreetmap. In *Proceedings of the 33rd ACM International Conference on Information and Knowledge Management*, pages 87–97, 2024.
- [3] JIANG Bohui and ZHOU Weifeng. Comparative analysis of geohash, google s2 and uber h3 as global geographic grid coding methods. *Geography & Geographic Information Science*, 40(2), 2024.
- [4] Maksym Bondarenko, David Kerr, Alessandro Sorichetta, and Andrew Tatem. Census/projection-disaggregated gridded population datasets, adjusted to match the corresponding unpd 2020 estimates, for 183 countries in 2020 using built-settlement growth model (bsgm) outputs. 2020.
- [5] Jianlv Chen, Shitao Xiao, Peitian Zhang, Kun Luo, Defu Lian, and Zheng Liu. Bge m3-embedding: Multi-lingual, multi-functionality, multi-granularity text embeddings through self-knowledge distillation, 2024.
- [6] Yile Chen, Weiming Huang, Kaiqi Zhao, Yue Jiang, and Gao Cong. Self-supervised representation learning for geospatial objects: A survey. *Information Fusion*, page 103265, 2025.
- [7] Jiawei Cheng, Jingyuan Wang, Yichuan Zhang, Jiahao Ji, Yuanshao Zhu, Zhibo Zhang, and Xiangyu Zhao. Poi-enhancer: An llm-based semantic enhancement framework for poi representation learning. In *Proceedings of the AAAI Conference on Artificial Intelligence*, volume 39, pages 11509–11517, 2025.
- [8] Shushman Choudhury, Elad Aharoni, Chandrakumari Suvarna, Ivel Tsogsuren, Abdul Rahman Kreidieh, Chun-Ta Lu, and Neha Arora. S2vec: Self-supervised geospatial embeddings. *arXiv preprint arXiv:2504.16942*, 2025.
- [9] Gordon Christie, Neil Fendley, James Wilson, and Ryan Mukherjee. Functional map of the world. In *Proceedings of the IEEE Conference on Computer Vision and Pattern Recognition*, pages 6172–6180, 2018.
- [10] Zhuangyuan Fan, Fan Zhang, Becky PY Loo, and Carlo Ratti. Urban visual intelligence: Uncovering hidden city profiles with street view images. *Proceedings of the National Academy of Sciences*, 120(27):e2220417120, 2023.
- [11] Jie Feng, Yuwei Du, Tianhui Liu, Siqi Guo, Yuming Lin, and Yong Li. Citygpt: Empowering urban spatial cognition of large language models. *arXiv preprint arXiv:2406.13948*, 2024.
- [12] Xiangnan He, Kuan Deng, Xiang Wang, Yan Li, Yongdong Zhang, and Meng Wang. Lightgcn: Simplifying and powering graph convolution network for recommendation. In *Proceedings of the 43rd International ACM SIGIR conference on research and development in Information Retrieval*, pages 639–648, 2020.
- [13] Tom Henighan, Jared Kaplan, Mor Katz, Mark Chen, Christopher Hesse, Jacob Jackson, Heewoo Jun, Tom B Brown, Prafulla Dhariwal, Scott Gray, et al. Scaling laws for autoregressive generative modeling. *arXiv preprint arXiv:2010.14701*, 2020.
- [14] Yingjing Huang, Fan Zhang, Yong Gao, Wei Tu, Fabio Duarte, Carlo Ratti, Diansheng Guo, and Yu Liu. Comprehensive urban space representation with varying numbers of street-level images. *Computers, Environment and Urban Systems*, 106:102043, 2023.
- [15] Jie Jiang, Lele Yu, Jiawei Jiang, Yuhong Liu, and Bin Cui. Angel: a new large-scale machine learning system. *National Science Review*, 5(2):216–236, 2018.
- [16] Jared Kaplan, Sam McCandlish, Tom Henighan, Tom B. Brown, Benjamin Chess, Rewon Child, Scott Gray, Alec Radford, Jeffrey Wu, and Dario Amodei. Scaling laws for neural language models, 2020. URL <https://arxiv.org/abs/2001.08361>.

- [17] Guolin Ke, Qi Meng, Thomas Finley, Taifeng Wang, Wei Chen, Weidong Ma, Qiwei Ye, and Tie-Yan Liu. Lightgbm: A highly efficient gradient boosting decision tree. In I. Guyon, U. Von Luxburg, S. Bengio, H. Wallach, R. Fergus, S. Vishwanathan, and R. Garnett, editors, *Advances in Neural Information Processing Systems*, volume 30. Curran Associates, Inc., 2017. URL https://proceedings.neurips.cc/paper_files/paper/2017/file/6449f44a102fde848669bdd9eb6b76fa-Paper.pdf.
- [18] Salman Khan, Muzammal Naseer, Munawar Hayat, Syed Waqas Zamir, Fahad Shahbaz Khan, and Mubarak Shah. Transformers in vision: A survey. *ACM computing surveys (CSUR)*, 54(10s):1–41, 2022.
- [19] Konstantin Klemmer, Esther Rolf, Caleb Robinson, Lester Mackey, and Marc Rußwurm. Satclip: Global, general-purpose location embeddings with satellite imagery. *Proceedings of the AAAI Conference on Artificial Intelligence*, 39(4):4347–4355, Apr. 2025. doi: 10.1609/aaai.v39i4.32457. URL <https://ojs.aaai.org/index.php/AAAI/article/view/32457>.
- [20] Zechen Li, Weiming Huang, Kai Zhao, Min Yang, Yongshun Gong, and Meng Chen. Urban region embedding via multi-view contrastive prediction. In *Proceedings of the AAAI Conference on Artificial Intelligence*, volume 38, pages 8724–8732, 2024.
- [21] Zekun Li, Jina Kim, Yao-Yi Chiang, and Muhao Chen. Spabert: a pretrained language model from geographic data for geo-entity representation. *arXiv preprint arXiv:2210.12213*, 2022.
- [22] Zekun Li, Wenxuan Zhou, Yao-Yi Chiang, and Muhao Chen. Geolm: Empowering language models for geospatially grounded language understanding. *arXiv preprint arXiv:2310.14478*, 2023.
- [23] Fan Liu, Delong Chen, Zhangqingyun Guan, Xiacong Zhou, Jiale Zhu, Qiaolin Ye, Liyong Fu, and Jun Zhou. Remoteclip: A vision language foundation model for remote sensing. *IEEE Transactions on Geoscience and Remote Sensing*, 62:1–16, 2024. doi: 10.1109/TGRS.2024.3390838. URL <https://doi.org/10.1109/TGRS.2024.3390838>.
- [24] Gengchen Mai, Krzysztof Janowicz, Bo Yan, Rui Zhu, Ling Cai, and Ni Lao. Multi-scale representation learning for spatial feature distributions using grid cells. In *The Eighth International Conference on Learning Representations*. openreview, 2020.
- [25] Gengchen Mai, Ni Lao, Yutong He, Jiaming Song, and Stefano Ermon. Csp: Self-supervised contrastive spatial pre-training for geospatial-visual representations. In *International Conference on Machine Learning*. PMLR, 2023.
- [26] Gengchen Mai, Yao Xuan, Wenyun Zuo, Yutong He, Jiaming Song, Stefano Ermon, Krzysztof Janowicz, and Ni Lao. Sphere2vec: A general-purpose location representation learning over a spherical surface for large-scale geospatial predictions. *ISPRS Journal of Photogrammetry and Remote Sensing*, pages 439–462, 2023.
- [27] Gengchen Mai, Weiming Huang, Jin Sun, Suhang Song, Deepak Mishra, Ninghao Liu, Song Gao, Tianming Liu, Gao Cong, Yingjie Hu, et al. On the opportunities and challenges of foundation models for geoi (vision paper). *ACM Transactions on Spatial Algorithms and Systems*, 10(2):1–46, 2024.
- [28] Gengchen Mai, Yiqun Xie, Xiaowei Jia, Ni Lao, Jimeng Rao, Qing Zhu, Zeping Liu, Yao-Yi Chiang, and Junfeng Jiao. Towards the next generation of geospatial artificial intelligence. *International Journal of Applied Earth Observation and Geoinformation*, 136:104368, 2025.
- [29] Ben Mildenhall, Pratul P. Srinivasan, Matthew Tancik, Jonathan T. Barron, Ravi Ramamoorthi, and Ren Ng. Nerf: Representing scenes as neural radiance fields for view synthesis. In *ECCV*, 2020.
- [30] National Bureau of Statistics of China. *China Statistical Yearbook 2020*. China Statistics Press, Beijing, China, 2020. URL <https://www.stats.gov.cn/sj/ndsj/2020/indexeh.htm>. Accessed May 15, 2025.

- [31] Alec Radford, Jong Wook Kim, Chris Hallacy, Aditya Ramesh, Gabriel Goh, Sandhini Agarwal, Girish Sastry, Amanda Askell, Pamela Mishkin, Jack Clark, Gretchen Krueger, and Ilya Sutskever. Learning transferable visual models from natural language supervision, 2021. URL <https://arxiv.org/abs/2103.00020>.
- [32] Esther Rolf, Jonathan Proctor, Tamma Carleton, Ian Bolliger, Vaishaal Shankar, Miyabi Ishihara, Benjamin Recht, and Solomon Hsiang. A generalizable and accessible approach to machine learning with global satellite imagery. *Nature Communications*, 12(1):4392, 2021. doi: 10.1038/s41467-021-24638-z.
- [33] Marc Rußwurm, Konstantin Klemmer, Esther Rolf, Robin Zbinden, and Devis Tuia. Geographic location encoding with spherical harmonics and sinusoidal representation networks. In *Proceedings of the International Conference on Learning Representations (ICLR)*, 2024. URL <https://iclr.cc/virtual/2024/poster/18690>.
- [34] Jian Tang, Meng Qu, Mingzhe Wang, Ming Zhang, Jun Yan, and Qiaozhu Mei. Line: Large-scale information network embedding. In *WWW*. ACM, 2015.
- [35] Tencent LBS Platform. Tencent map poi web service guide. <https://lbs.qq.com/service/webService/webServiceGuide/webServiceAppendix>, 2024. Accessed: 2025-05-16.
- [36] Uber Technologies, Inc. H3: Hexagonal hierarchical geospatial indexing system. <https://h3geo.org/>. Accessed: 2025-05-04.
- [37] Grant Van Horn, Oisin Mac Aodha, Yang Song, Yin Cui, Chen Sun, Alex Shepard, Hartwig Adam, Pietro Perona, and Serge Belongie. The inaturalist species classification and detection dataset. In *Proceedings of the IEEE conference on computer vision and pattern recognition*, pages 8769–8778, 2018.
- [38] Vicente Vivanco, Gaurav Kumar Nayak, and Mubarak Shah. Geoclip: Clip-inspired alignment between locations and images for effective worldwide geo-localization. In *Advances in Neural Information Processing Systems*, 2023.
- [39] Hongjian Wang and Zhenhui Li. Region representation learning via mobility flow. In *Proceedings of the 2017 ACM on Conference on Information and Knowledge Management, CIKM '17*, page 237–246, New York, NY, USA, 2017. Association for Computing Machinery. ISBN 9781450349185. doi: 10.1145/3132847.3133006. URL <https://doi-org.eproxy.lib.hku.hk/10.1145/3132847.3133006>.
- [40] Ya Wen and Yulun Zhou. Demo2vec: Learning region embedding with demographic information. In *Proceedings of the 7th ACM SIGSPATIAL International Workshop on AI for Geographic Knowledge Discovery*, pages 71–74, 2024.
- [41] Szymon Woźniak and Piotr Szymański. Hex2vec: Context-aware embedding h3 hexagons with openstreetmap tags. In *Proceedings of the 4th ACM SIGSPATIAL International Workshop on AI for Geographic Knowledge Discovery*, pages 61–71, 2021.
- [42] Nemin Wu, Qian Cao, Zhangyu Wang, Zeping Liu, Yanlin Qi, Jielu Zhang, Joshua Ni, X. Angela Yao, Hongxu Ma, Lan Mu, Stefano Ermon, Tanuja Ganu, Akshay Nambi, Ni Lao, and Gengchen Mai. Torchspatial: A location encoding framework and benchmark for spatial representation learning. In *The Thirty-eight Conference on Neural Information Processing Systems Datasets and Benchmarks Track*, 2024. URL <https://openreview.net/forum?id=DERtzUdhkk>.
- [43] Shangbin Wu, Xu Yan, Xiaoliang Fan, Shirui Pan, Shichao Zhu, Chuanpan Zheng, Ming Cheng, and Cheng Wang. Multi-graph fusion networks for urban region embedding. *arXiv preprint arXiv:2201.09760*, 2022.
- [44] WorldPop (www.worldpop.org School of Geography, University of Southampton; Department of Geography Environmental Science, Universite de Namur) Geosciences, University of Louisville; Departement de Geographie, and Columbia University Center for International Earth Science Information Network (CIESIN). Global high resolution population denominators project, 2018. URL <https://dx.doi.org/10.5258/SOTON/WP00646>. Funded by The Bill and Melinda Gates Foundation (OPP1134076).

- [45] Congxi Xiao, Jingbo Zhou, Yixiong Xiao, Jizhou Huang, and Hui Xiong. Refound: Crafting a foundation model for urban region understanding upon language and visual foundations. In Proceedings of the 30th ACM SIGKDD Conference on Knowledge Discovery and Data Mining, KDD '24, page 3527–3538, New York, NY, USA, 2024. Association for Computing Machinery. ISBN 9798400704901. doi: 10.1145/3637528.3671992. URL <https://doi-org.eproxy.lib.hku.hk/10.1145/3637528.3671992>.
- [46] Zhuo Xu and Xiao Zhou. Cgap: urban region representation learning with coarsened graph attention pooling. arXiv preprint arXiv:2407.02074, 2024.
- [47] Yibo Yan, Haomin Wen, Siru Zhong, Wei Chen, Haodong Chen, Qingsong Wen, Roger Zimmermann, and Yuxuan Liang. Urbanclip: Learning text-enhanced urban region profiling with contrastive language-image pretraining from the web. In Proceedings of the ACM Web Conference 2024, pages 4006–4017, 2024.
- [48] Christopher Yeh, Anthony Perez, Anne Driscoll, George Azzari, Zhongyi Tang, David Lobell, Stefano Ermon, and Marshall Burke. Using publicly available satellite imagery and deep learning to understand economic well-being in africa. Nature communications, 11(1):2583, 2020.
- [49] Yifang Yin, Zhenguang Liu, Ying Zhang, Sheng Wang, Rajiv Ratn Shah, and Roger Zimmermann. Gps2vec: Towards generating worldwide gps embeddings. In Proceedings of the 27th ACM SIGSPATIAL International Conference on Advances in Geographic Information Systems, pages 416—419, 2019.
- [50] Yifang Yin, Ying Zhang, Zhenguang Liu, Yuxuan Liang, Sheng Wang, Rajiv Ratn Shah, and Roger Zimmermann. Learning multi-context aware location representations from large-scale geotagged images. In Proceedings of the 29th ACM International Conference on Multimedia, pages 899—907, 2021.
- [51] Xixian Yong and Xiao Zhou. Musecl: Predicting urban socioeconomic indicators via multi-semantic contrastive learning. arXiv preprint arXiv:2407.09523, 2024.
- [52] Liang Zhang, Cheng Long, and Gao Cong. Region embedding with intra and inter-view contrastive learning. IEEE Transactions on Knowledge and Data Engineering, 35(9):9031–9036, 2022.
- [53] Mingyang Zhang, Tong Li, Yong Li, and Pan Hui. Multi-view joint graph representation learning for urban region embedding. In Proceedings of the twenty-ninth international conference on international joint conferences on artificial intelligence, pages 4431–4437, 2021.
- [54] Weijia Zhang, Jindong Han, Zhao Xu, Hang Ni, Hao Liu, and Hui Xiong. Towards urban general intelligence: A review and outlook of urban foundation models. arXiv preprint arXiv:2402.01749, 2024.
- [55] Yan Zhang, Mei-Po Kwan, and Libo Fang. A llm driven dataset on the spatiotemporal distributions of street and neighborhood crime in china, 2025. URL <https://doi.org/10.6084/m9.figshare.28106855.v1>. Dataset.
- [56] Silin Zhou, Dan He, Lisi Chen, Shuo Shang, and Peng Han. Heterogeneous region embedding with prompt learning. In Proceedings of the AAAI conference on artificial intelligence, volume 37, pages 4981–4989, 2023.

A Appendix

A.1 Detailed Implementation of the Distillation

For model distillation, we fit a surrogate Multi-Layer Perceptron (MLP) network to estimate pretrained region embeddings from MobCLIP. For each H3 cell, the input for the MLP is a 1024-d vector, which is a SIREN encoding [33] of the centroid coordinate of the cell. The output for the MLP is a 128-d vector from MobCLIP. The MLP is configured with 8 hidden layers, with a dimension of 512 each. The model is trained with an MSE loss function to minimize the deviation of estimated embeddings from our true embeddings. The learning rate is set to 0.005 for 5000 epochs. Final training loss is 0.0857. The downstream performance of the distilled model is shown in Table 3. Note that the performance of the distilled model (MobCLIP_d) tends to improve as the number of MLP layers and the size of the hidden dimensions increase. We here demonstrate the distillation effectiveness preliminarily using the model size mentioned above.

Table 3: Performance comparison between MobCLIP_d and baselines.

	Social Tasks					Economic Tasks			Natural Tasks		
	POP	EDU	ELD	HSR	CRI	NTL	HOU	ENE	COS	ELE	FOR
SatCLIP	0.523	0.633	0.676	0.735	0.391	0.334	0.655	-0.069	0.443	0.963	0.806
MobCLIP	0.829	0.853	0.812	0.810	0.759	0.615	0.703	0.719	0.909	0.900	0.797
MobCLIP _d	0.730	0.835	0.804	0.816	0.580	0.517	0.693	0.742	0.729	0.906	0.785

A.2 Results Table for the Scaling Behavior

Table 4: Downstream Task Performance (R²) Under Model Variants in Scaling Behavior.

	Jiangsu	East China	China
Social			
POP	0.675	0.746	0.755
EDU	0.753	0.840	0.817
ELD	0.551	0.724	0.748
HSR	0.809	0.883	0.858
CRI	0.743	0.748	0.750
Economic			
NTL	0.547	0.551	0.616
HOU	0.529	0.648	0.581
ENE	0.733	0.810	0.889
COS	0.846	0.861	0.891

A.3 Sensitivity to H3 Grid Resolution

We extend our study at H3 resolution level 6 to its adjacent levels, 5 and 7, to evaluate the model’s performance across different spatial scales. Compared to level 6 H3 cells, which cover an average area of 36.13 km², cells at levels 5 and 7 cover approximately 253.61 km² and 5.18 km², respectively. The East China region is selected for testing to facilitate ease of operation without losing generalizability. We reconstruct the training dataset for levels 5 and 7 from scratch, including forming trajectory-based mobility graphs, gathering satellite imagery and POIs for encodings, and processing demographic distributions data. Three separate experiments are conducted, with corresponding sets of downstream data processed for evaluation. Since cities in East China are limited in quantity, we choose Ridge Regression for electricity prediction across all levels to ensure consistency. For the remaining tasks, LightGBM is adopted. Table 5 demonstrates the model’s performance with varying resolutions. For grid-level predictions, the performance tends to decline as the level of granularity increases. This is because, at finer resolutions, the data becomes more heterogeneous and exhibits greater variations. However, an exception is observed with population prediction, which follows a reversed pattern.

Table 5: Sensitivity of model performance using different grid resolutions.

	NTL	Grid-level			EDU.	County-level			City-level
		COS	CRI.	POP.		ELD.	HOU.	MIG.	ELE.
H3 lv5	0.462	0.881	0.838	0.679	0.645	0.668	0.611	0.830	0.659
H3 lv6	0.632	0.901	0.764	0.817	0.790	0.698	0.665	0.835	0.668
H3 lv7	0.741	0.934	0.634	0.836	0.821	0.754	0.700	0.872	0.711

This might be explained by the fact that population is a localized variable that demonstrates stronger patterns at smaller spatial scales. On the other hand, aggregating spatial units smooths out local fluctuations and emphasizes important features in the embedding, as evidenced by the improvement in the model’s performance on county- and city-level tasks with higher resolution levels.